DOI: https://doi.org/10.71317/kjard.2.10.2026. 920

Kashmir Journal of Academic Research and Development

Journal homepage: https://rjsaonline.org/index.php/KJARD

Numerical and Experimental Assessment of Dual-Surface Triangular Roughness on the Aerodynamic Performance of a CR001SM Airfoil

Fayaz Ahmed
Department of Mechanical Engineering Technology, The Benazir Bhutto Shaheed University of Technology and Skills Development, Khairpur Mirs
Email: Fayaz.24ms-met-06@bbsuted.edu.pk
Ali Mustafa Shah
Department of Mechanical Engineering Technology, The Benazir Bhutto Shaheed University of Technology and Skills Development, Khairpur Mirs
Email: mustafa@bbsutsd.edu.pk
Asif Ali
Department of Mechanical Engineering, The University of Larkano
Email: asifali@uolrk.edu.pk
Sajjad Bhangwar
Department of Mechanical Engineering, Quaid-e-Awam University of Engineering Science and Technology
Email: Sajjadbhangwar@quest.edu.pk
Athar Ali Khan Gorar
Department of Mechanical Engineering, The University of Larkano
Email: atahar_gorar@hotmail.com

ARTICLE INFO

Received:
September 15, 2026
Revised:
October 14, 2026
Accepted:
October 20, 2026
Available Online:
October 27, 2026

Keywords:
CR001SM airfoil, triangular roughness, passive flow control, low Reynolds number, aerodynamic performance.

Corresponding Author:
Fayaz Ahmed
Email:
Fayaz.24ms-met06@bbsuted.edu.pk

ABSTRACT

Passive flow-control techniques are crucial to enhancing the performance of airfoils at low Reynolds numbers, where boundary-layer separation and related aerodynamic losses are a problem. This study examines the aerodynamic performance of a CR001SM airfoil with both upper and lower surface triangular roughness elements at low Reynolds numbers. Two modified configurations were tested: M1 (roughness elements at 5% and 80% of the chord) and M2 (roughness elements at 10% and 70% of the chord). Experimental wind-tunnel measurements and numerical simulations were carried out in ANSYS Fluent 2021 R1 with the transient Transition SST model to compare the aerodynamic characteristics of these configurations with that of the smooth baseline airfoil. Freestream velocities of 1.25 m/s, 2.25 m/s and 3.0 m/s and angles of attack between 0^{o} and 18^{o} were investigated. The lift, drag and aerodynamics are strongly affected by the roughness configuration. The maximum lift coefficient of M1 is around 1.19, 1.24 and 1.28 at 1.25, 2.25 and 3.0 m/s respectively. The smooth airfoil, on the other hand, has a lower drag and thus better lift-to-drag ratio at low and moderate angles of attack. The roughened configurations have relatively good lift retention at higher angles of attack, and at some angles of attack, lower drag than the smooth airfoil. The overall average absolute percentage deviation obtained from the numerical validation is around 8.79% with experimental lift coefficients. The aerodynamic effects of triangle roughness are influenced by the angle of attack, freestream velocity, and chordwise location of the triangle. The M1 configuration is beneficial in situations where high angle of attack lift retention is important.

Introduction

In aerodynamics, airfoils are a basic element that is extensively employed in engineering systems such as aircraft wings, wind turbines, propellers and unmanned aerial vehicles (UAVs) [1]. The aerodynamic performance is highly dependent on the

behavior of the boundary layer, especially the separation, transition and stall [2]. These effects are more sensitive at lower Reynolds numbers, where the boundary layer is more likely to separation with adverse pressure gradients. In the aerodynamic design of low-Reynolds-number airfoils, therefore, it is important to delay flow separation and stall, especially for UAV and other small-scale aerodynamic applications [3][4]. To overcome these aerodynamic problems, several flow-control methods have been developed to alter the behavior of the boundary layer and enhance the aerodynamic performance [5][5][6][7]. There are two basic types of flow-control techniques: active and passive [8][9][10]. Active flow-control methods like suction, blowing, synthetic jets, plasma actuators, acoustic excitation and oscillatory devices have shown significant promise when it comes to delaying the beginning of flow separation, laminar separation bubbles and lift enhancement [8][11] [12][13]. In general, they need external power sources, sensors, actuators and control systems, which makes the system more complex, costly in and heavier [6].

Passive flow control techniques, on the other hand, have been shown to be an alternative since they change the flow field by using fixed geometric features without the need for external energy input or complex control systems [9][14][15]. Contrary, passive flow deflectors have been studied to change the near wall flow and delay flow separation [6]. Numerical optimization of leading edge flow deflectors was performed by Xu et al. [5] by using Computational Fluid Dynamics (CFD) and the Efficient Global Optimization (EGO) algorithm. The optimized passive deflector resulted in a 58.37% increase in the lift coefficient from 0.785 to 1.24 for a NACA 0012 airfoil at an angle of attack of 19°, and a 13.59% decrease in the drag coefficient from 0.288 to 0.249. As a result, the lift-to-drag ratio improved from 2.721 to 4.987, which is an increase of 83.29%, and the stall angle was delayed by about 7°. The sensitivity analysis also showed that the aerodynamic performance was affected significantly by the geometric parameters.

Similarly, cavity-based airfoils and surface roughness, have also been investigated for controlling flow separation. The cavity produces counter-rotating vortices, which change the pressure distribution around the suction surface. Olsman and Colonius [16] numerically studied a cavitied airfoil at Re (2×10^4) and found that the separated flow region in the cavity can be reduced and stall delayed due to the counter-rotating flow generated within the cavity. The aerodynamic efficiency, however, especially the lift to drag ratio over a wide range of angles of attack was not sufficiently determined. Similarly, Lam and Leung [17], results indicated that the cavities configuration generated lower acoustic power than the baseline airfoil, suggesting potential benefits for low-Reynolds-number applications, it enhances the lift-to-drag ratio of airfoil. Another passive way of controlling the behavior of the boundary layer is through surface roughness. The proper design of roughness elements can create vertical structures near the wall, which can increase the momentum transfer between the outer flow and the boundary layer [18]. This extra momentum can help to reduce the susceptibility of the boundary layer to adverse pressure gradients and therefore delay or prevent flow separation [2][19]. However, the effectiveness of roughness is very sensitive to its geometry, size, location, Reynolds number, and flow conditions. Several previous passive control experiments reported by the authors such as 17.7–21.4% drag reduction with miniature cylinders, 4.61% drag reduction with slat-gaps, and 10–30% C_L/C_D improvement with needle-vortex-generator [20]. Likewise, it is reported that the use of dimple vortex generators can create streamwise vortices which improve flow reattachment, decrease drag and significantly increase the lift-to-drag ratio [15][21]. In addition, slotted airfoils have been shown to have excellent re-energizing and stall delay characteristics over a broad range of operating conditions [3][4]. All of these studies show that passive flow control can provide aerodynamic benefits that are similar to many active control methods without the drawbacks of external power sources and control systems[1][11].

Although passive flow control techniques have been extensively studied, there are still several important gaps in the understanding of roughness based flow control at low Reynolds numbers. The vortex generators, dimples, slots, cavities, riblets, and leading edge modifications have been the focus of most previous studies, whereas comparatively few studies have been conducted on systematically designed triangular roughness elements [21][22][23][24]. Furthermore, most of the previous studies have focused on the modification of the roughness on a single surface of the airfoil. The simultaneous application of the aerodynamic effects of the two triangular roughness elements on the top and bottom surfaces is still not well understood. The effects of dual surface roughness on boundary layer development, pressure distribution, flow separation, laminar separation bubbles, lift, drag and aerodynamic efficiency at low Reynolds numbers have not been sufficiently investigated [1][24][20]. In the present study, the aerodynamic performance of a low-Reynolds-number airfoil with triangular upper and lower surface roughness elements is experimentally and numerically studied. The effects of the roughness configuration are investigated at a range of angles of attack through the analysis of the lift coefficient (C_L), drag coefficient (C_D), lift-to-drag ratio (C_L/C_D) and flow separation characteristics. The study also investigates the changes in the near wall flow and pressure distribution when the roughness elements are added and placed on the airfoil versus the baseline airfoil.

Materials and Methods

Airfoil Geometry and Triangular Roughness Configuration

The CR001SM airfoil was chosen as the baseline airfoil for the present study due to its relevance in small-scale, low-speed aerodynamic applications. The airfoil has a chord length of 160 mm (0.160 m). The baseline configuration was a smooth CR001SM airfoil, while the upper and lower surfaces modified by adding triangular roughness elements. The triangular roughness elements were fixed geometric surface modifications that were designed to change the near-wall flow and boundary-layer development. The roughness elements were placed at the desired chordwise locations from the leading edge as shown in Table 1. Physical models of bassline and modified airfoils were made by CNC machining at the department of mechanical engineering, The University of Larkano, Larkana using acrylic material. The holes were then pressure-tapped at the indicated points on the top and bottom surfaces for experimental pressure measurements.

Table 1; Airfoil model configuration.

Model	Upper-surface roughness location	Lower-surface roughness location	No. of triangular elements
Baseline	None	None	None
M_1	5 % C	80 %C	5
M_2	10 %C	70%C	5

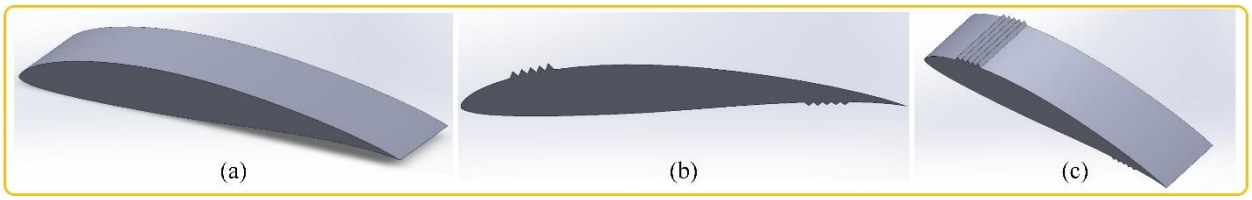


Figure 1. Airfoil model (a) Baseline (b) M_1 and (c) M_2.

Wind-Tunnel Experimental Setup and Measurement Procedure

Experimental investigation was carried out in the Aerodynamics Laboratory of Department of Mechanical Engineering, QUEST, Nawabshah in a subsonic wind tunnel. The test section is 50 × 250 mm and the airflow was produced by a variable speed fan, experiments were conducted at the velocities of about 1.25–3.0 m/sec. These conditions are used to obtain the low Reynolds number flow regime of the present study. The airfoil model CR001SM was secured in the test section, and the pressure taps were placed on the upper and lower surface of the airfoil and connected to a multi-tube manometer. The levels of the manometer were checked and adjusted before each measurement to establish the reference condition. The wind tunnel fan then started and the flow was allowed to stabilize, and the pressures at each of the pressure taps were recorded. The measurements were conducted at the angles of attack from 0° to 18° and flow velocities (1.25–3.0 m/sec) for both the baseline and modified airfoil configurations. The water manometer was used to measure the difference in pressure at various points along the surface of the airfoil, and the pressure distribution over the surface was determined. The local pressure coefficient was calculated as;

$$C_p = \frac{P - P_\infty}{\frac{1}{2}\rho U_\infty^2} \qquad 1$$

where P, P_∞, ρ, and U_∞ are the local static pressure at the pressure tap, the freestream static pressure, the air density, and the freestream velocity, respectively. Lift coefficient was calculated from the pressure distribution on the upper and lower surfaces for the two-dimensional airfoil. The pressure coefficient distributions were numerically integrated using trapezoidal integration method.

$$C_L = \int_0^1 C_{p,L}\ d(x/c) - \int_0^1 C_{p,U}\ d(x/c) \qquad 2$$

where $C_{p,L}$ and $C_{p,U}$ are the pressure coefficients on the lower and upper surface, respectively. The lift coefficient was thus directly determined from the measured surface pressure distribution by using trapezoidal integration method, and this approach was used for experimental investigation.

Computational Domain and Mesh Generation

A C-shaped computational domain was used for the numerical investigation of the two-dimensional CR001SM airfoil. The computational domain was large enough upstream and downstream of the airfoil to reduce the effect of the outer boundaries on the numerical simulation. Around the airfoil a structured body-fitted mesh was created, mostly made up of quadrilaterals. Local mesh refinement was performed near the airfoil surface and especially around the triangular roughness elements to capture the high velocity and pressure gradients in these areas. Additionally, near-wall refinement was used to achieve a proper capture of the boundary-layer development. The mesh was developed and the Transition SST model was used for simulation. The computational domain was created as a 2-D C-shaped domain with a body-fitted mesh around the airfoil. The final mesh was composed of 240,000 elements and 240,960 nodes. The average and maximum skewness were 0.069 and 0.878, respectively, which were acceptable. The boundary layer flow was resolved by local refinement near the surface of the airfoil and near the triangular roughness elements.

CFD Methodology and Boundary Conditions

Numerical simulation was carried out by using the ANSYS 2021 R1. The Fluent solver configuration was used, and a pressure based, transient solver with a two dimensional planar design was used. The flow was assumed to be incompressible as the test velocities were relatively low (1.25 to 3.0 m/sec). A model called the Transition SST model was used to simulate the separated-flow and boundary layer transition phenomena. The model was chosen because the present investigation is concerned with low Reynolds number flow where the interaction between laminar boundary layers, transition and flow separation is of importance. The computational domain included an inlet, an outlet, and solid wall for the external flow boundaries that were selected. The freestream velocity was set at the inlet, and the outlet was specified by a pressure-outlet condition. The airfoil surface was assumed to be a no slip surface. In order to make a direct comparison between the numerical and experimental results, the same geometric configurations used in the experimental investigation were reproduced in the CFD model. The simulations were carried out for the chosen velocities and angles of attack. In each case, the transient solution was integrated to a statistically stable flow-field and aerodynamic force coefficients. The time-dependent aerodynamic forces on the airfoil were used to calculate the final lift and drag coefficients.

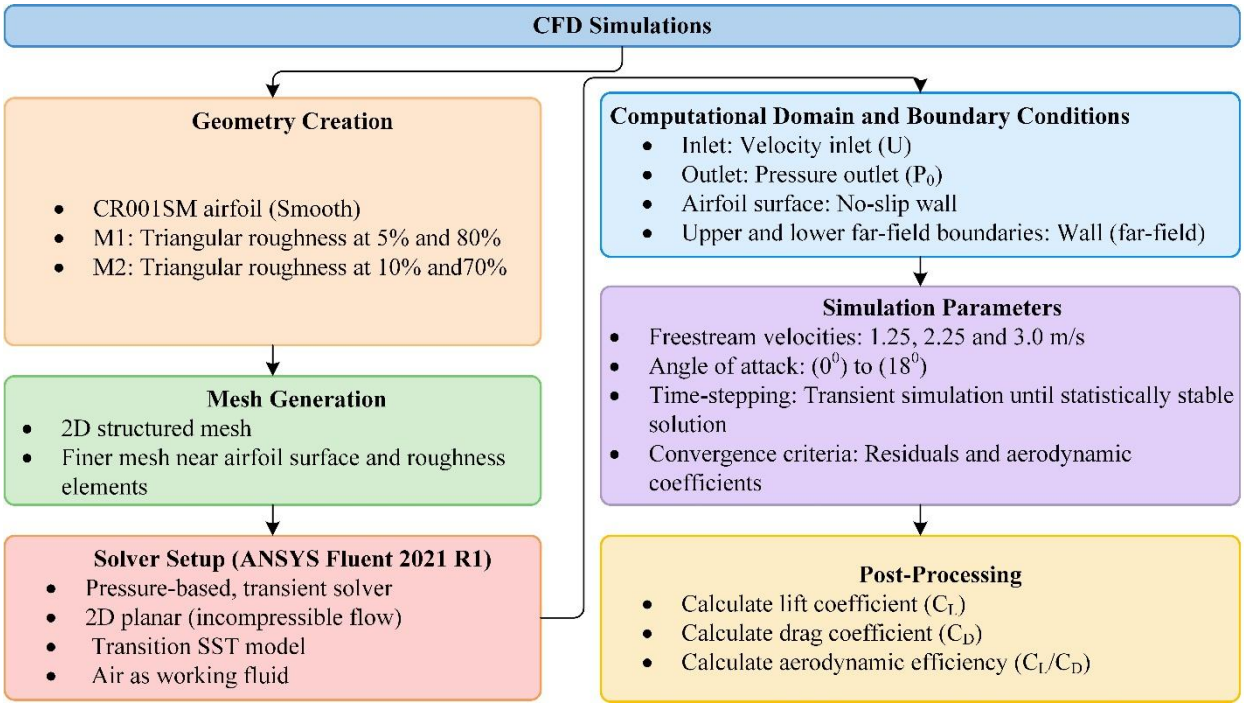


Figure 2. CFD simulation Methodology and Boundary Conditions.

Validation of Simulation results

As seen in Figure 3, the overall trend of the numerical results is in good agreement with the experimental results, such as the increase in lift as angle of attack increases, the region of maximum lift, and the decrease in lift at higher angles of attack. The average absolute errors for M1 airfoil are 6.17%, 7.05% and 8.36% at 1.25 m/sec, for M1, M2 and smooth respectively. The

overall average absolute error is about 7.20% for all experimental data points. The overall deviation is relatively small, which means that there is a good agreement between the numerical and experimental results. The greater variations in these areas close to the maximum lift and post-stall regions are due to the complex separated flow and transition phenomena of low Reynolds number aerodynamics.

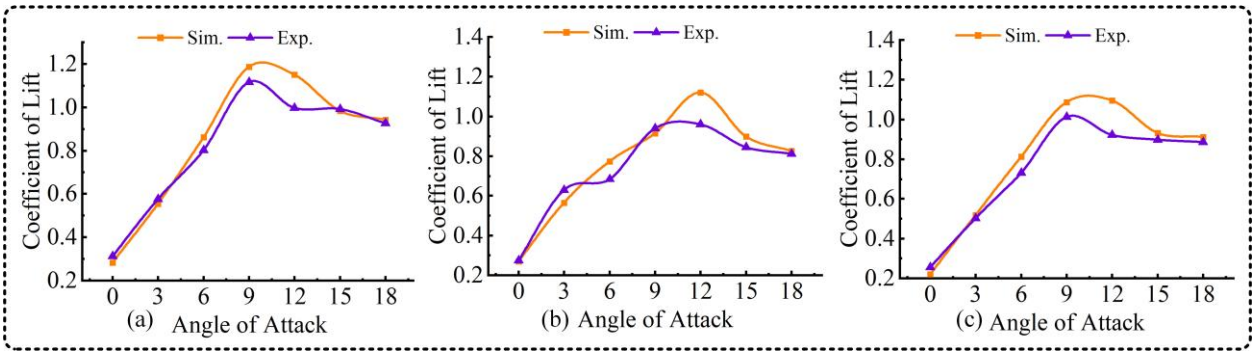


Figure 3.Comparison of coefficient of lift vs angle of attack at velocity of 1.25 m/sec, (a) M1 (b) M2 and (c) Smooth.

Results and Discussion

The numerical model was validated with the experimental measurements and the aerodynamic performance of the baseline CR001SM airfoil, and the two modified configurations (M_1 and M_2) was studied. The influence of the roughness configuration and freestream velocity was assessed by the lift coefficient (C_L), drag coefficient (C_D), and aerodynamic efficiency (C_L/C_D) at different angles of attack from 0° to 18°. Figure 4 shows the change in C_L with angle of attack for the freestream velocities investigated. The M_1 configuration has the highest simulated C_L equal to 1.187 at 9°, while M_2 and the smooth airfoil have approximately 1.120 and 1.095 respectively. At 18° M_1 maintains a C_L of 0.943, compared with 0.826 for M_2 and 0.913 for the smooth airfoil. So, M_1 has better lift retention at high angles of attack. The performance of all configurations increases at 2.25 m/sec. M_1 will have a C_L of 1.235 at 12°, while, M_2 will have a C_L of 1.124 at 12° and the smooth airfoil will have a C_L of 1.136 at 12°. M_1 still has the highest lift coefficient of 1.052, while M_2 has 0.986 and the smooth airfoil a 0.976 at 18°. The same general trend is seen at 3.0 m/sec. The highest C_L is obtained with M_1, around 11° – 12°, and is closely followed by M_2, with the smooth airfoil getting about 1.17. These results show that the C_L generation of the M_1 configuration is the best one of the roughness configurations investigated, especially at moderate and high angles of attack. The improved lift performance of M_1 compared with M_2 indicates that the chordwise placement of the roughness elements is an important parameter. The two configurations have triangular roughness on the upper and lower surfaces but the change in location from 5–80% chord to 10–70% chord causes a noticeable change in C_L characteristics.

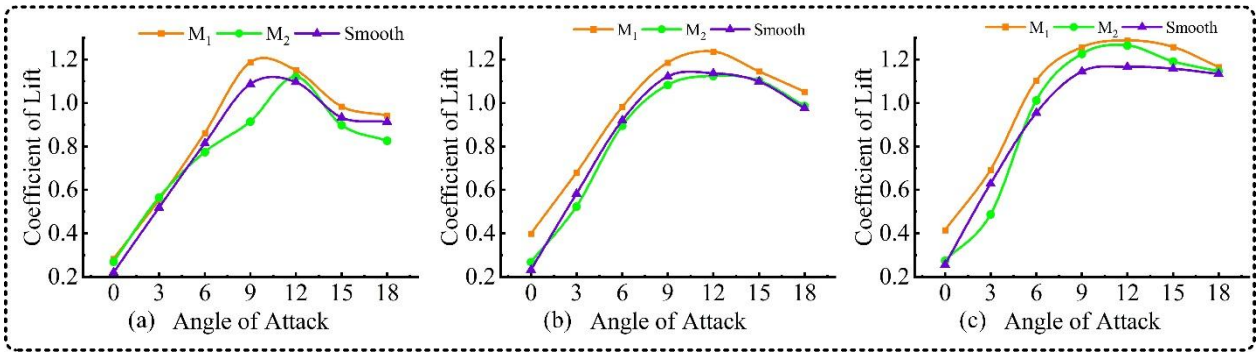


Figure 4. Coefficient of lift vs angle of attack at different velocities, (a) 1.25 m/sec, (b) 2.25 m/sec and (c) 3 m/sec.

All configurations and velocities see an increase in drag coefficient with the angle of attack, as shown in Figure 5. The roughened configurations typically have higher drag than the smooth airfoil at low and moderate angles of attack at 1.25 m/sec. For example, at 6°, the C_D values are 0.0934 for M_1, 0.1130 for M_2, and 0.0610 for the smooth airfoil. However, the drag of the smooth airfoil rises more quickly at higher angles of attack. At 18°, the simulated drag coefficients at 1.25 m/sec are 0.211 for M_1, 0.229 for M_2, and 0.254 for the smooth airfoil. This is also seen at 2.25 and 3.0 m/sec, with the smooth airfoil having a significant rise in drag at high angles of attack. This behavior shows that the roughened airfoil has more drag at low angles of

attack, but the behavior at high angles of attack can be modified and the rapid drag increase seen for the smooth airfoil is reduced. This effect is configuration dependent and M_1 tends to have a better drag response than M_2.

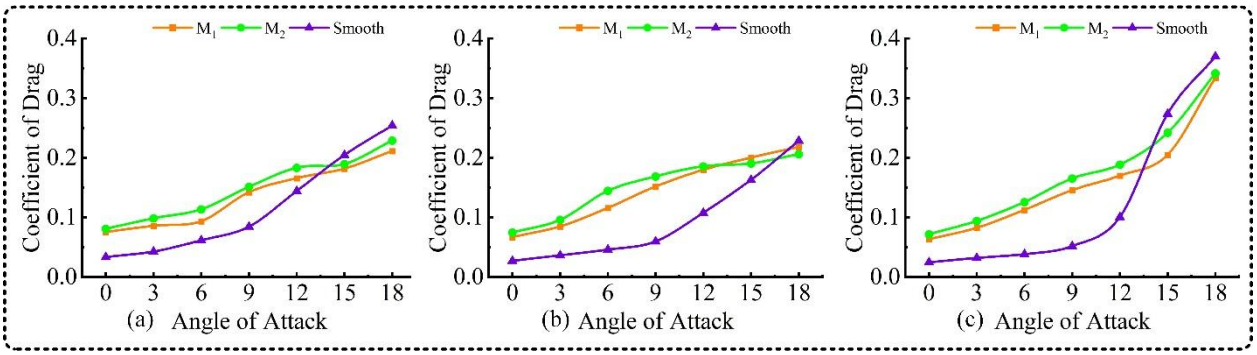


Figure 5. Coefficient of Drag vs angle of attack at different velocities, (a) 1.25 m/sec, (b) 2.25 m/sec and (c) 3 m/sec.

The variation of C_L/C_D shows the balance between the lift enhancement and drag penalty of the triangular roughness elements. The smooth airfoil offers the highest aerodynamic efficiency at 1.25 m/sec, with a C_L/ C_D of 13.33 at 6°, while M_1 and M_2 have C_L/ C_D of 9.23 and 6.85, respectively. The maximum C_L/ C_D of the smooth airfoil is about 20.18 at 6° when the velocity is 2.25 m/s. At 6°, the values of M_1 and M_2 are about 8.48 and 6.42, respectively. Thus, the smooth airfoil is still more aerodynamic at low to moderate angles of attack. The difference between the configurations is less at higher angles of attack. At 2.25 m/sec and 18°, the C_L/ C_D values are approximately 4.82 for M_1, 4.80 for M_2, and 4.28 for the smooth airfoil. This means that the roughened forms are more competitive in the high angle of attack regime, mainly due to their better lift retention and the relatively high rate of drag rise of the smooth airfoil.

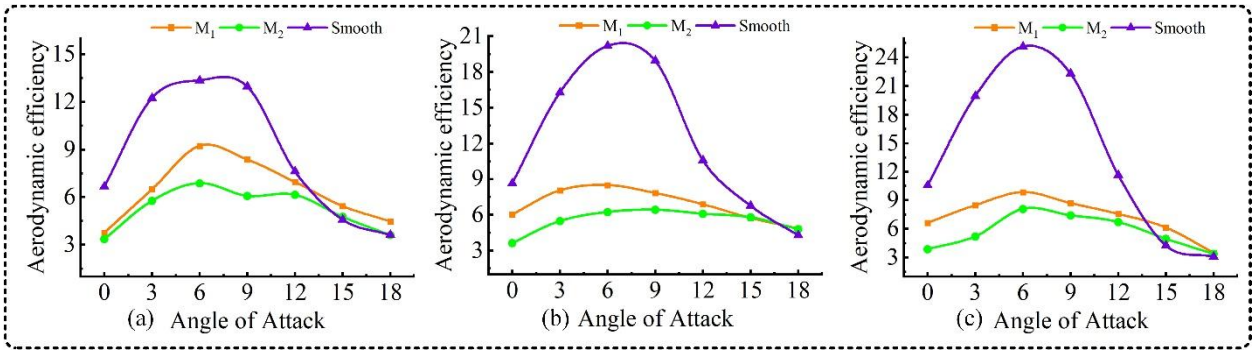


Figure 6. Aerodynamic performance of airfoil vs angle of attack at different velocities, (a) 1.25 m/sec, (b) 2.25 m/sec and (c) 3 m/sec.

Generally, the aerodynamic response of the airfoil configurations is better when the freestream velocity is increased from 1.25 to 3.0 m/sec. As the velocity increases, which causes changes in the behavior of the boundary layer and flow separation. This effect is more pronounced in the lift properties. M_1 raises its max simulated C_L from 1.19 at 1.25 m/sec to 1.24 at 2.25 m/sec and 1.28 at 3.0 m/sec. The maximum lift of the smooth airfoil also rises as velocity increases. This means that the aerodynamic response is becoming more positive with increasing Reynolds number. The comparison between M_1 and M_2 shows that it is not enough to just add roughness to the airfoil surface, but it is also important to consider the location of the roughness. In general, M_1 has higher coefficient of lift than M_2. At 2.25 m/sec, M_1 produces C_L (1.235) at 12° compared with 1.124 for M_2. At 18°, M_1 maintains C_L at 1.052, compared with 0.986 for M_2. The results indicate that the M_1 configuration offers a better overall aerodynamic response, especially in terms of lift retention at moderate and high angles of attack. The smooth airfoil is still the most desirable shape for a maximum aerodynamic efficiency at low to moderate angles of attack.

Conclusions

In this study, the aerodynamic behavior of a CR001SM airfoil with triangular roughness elements on the top and bottom surfaces was studied numerically and validated experimentally. The results show that the aerodynamic performance is dependent on the placement of the roughness, freestream velocity and angle of attack. In comparison with the other modified configurations, M_1 typically generated higher lift coefficients and maintained the lift at higher angles of attack than M_2 and smooth airfoil. The maximum simulated lift coefficients for M_1 were about 1.19, 1.24 and 1.28 at freestream velocities of 1.25, 2.25 and 3.0 m/sec respectively. The smooth airfoil, however, had a higher C_L/C_D ratio at low and moderate angles of attack due to its lower drag.

The roughened shapes had lower drag at higher angles of attack than the smooth baseline. The overall average absolute percentage difference between the numerical and experimental lift coefficient was about 8.79%, which shows good agreement between the two methods. In summary, M_1 is a good choice for applications where better lift retention is desired.

References

A. Krishnan, A. S. M. Al-obaidi, and L. C. Hao, "Review article A comprehensive review of innovative wind turbine airfoil and blade designs : Toward enhanced efficiency and sustainability," *Sustain. Energy Technol. Assessments*, vol. 60, no. October, p. 103511, 2023, doi: 10.1016/j.seta.2023.103511.

T. Bai, J. Liu, W. Zhang, and Z. Zou, "Effect of surface roughness on the aerodynamic performance of turbine blade cascade," *Propuls. Power Res.*, vol. 3, no. 2, pp. 82–89, Jun. 2014, doi: 10.1016/j.jppr.2014.05.001.

M. A. Aziz, M. A. Khalifa, M. A. Abdelrahman, H. Elshimy, and A. M. Elsayed, "Multi-slotted airfoil design for enhanced aerodynamic performance and economic efficiency," *Sci. Rep.*, vol. 15, no. 1, pp. 1–18, 2025, doi: 10.1038/s41598-025-87000-z.

H. E. Tanürün, A. Yıldız, and M. Seyhan, "Aerodynamic performance analysis of a NACA 63(4)-421 airfoil equipped with a trailing edge slot at suction side," *Exp. Therm. Fluid Sci.*, vol. 171, no. May 2025, p. 111604, Jan. 2026, doi: 10.1016/j.expthermflusci.2025.111604.

J. LI, S. XIE, and X. CHEN, "Impact of corrugated structures on airfoil aerodynamic performance," *Chinese J. Aeronaut.*, vol. 38, no. 10, p. 103534, 2025, doi: 10.1016/j.cja.2025.103534.

S. Xu, S. Wang, H. Chen, J. Tan, W. Li, and S. Yin, "Flow Separation Delay Mechanism and Aerodynamic Enhancement via Optimized Flow Deflector Configurations," *Actuators*, vol. 14, no. 9, pp. 1–19, 2025, doi: 10.3390/act14090428.

A. A. Laghari and M. A. Khoso, "Role of single bump over the surface of E398 Airfoil to improve the aerodynamic performance," *nternational J. Adv. Res. Ideas Innov. Technol.*, vol. 4, no. 4, pp. 550–556, 2018, [Online].

N. ÜNAL, Y. ÖZ, E. A. ÜNAL, and T. OKTAY, "Enhancing aerodynamic performance of a two-dimensional airfoil using plasma actuators," *Aerosp. Sci. Technol.*, vol. 158, no. October 2024, 2025, doi: 10.1016/j.ast.2024.109882.

J. Ma, Q. Li, M. Zhao, Y. Chen, and X. Chai, "A Passive Flow Control Technique of a Small-Scale HAWT and TED Analysis Under Yaw Condition Based on Airfoil Concavity," *Energies*, vol. 17, no. 24, 2024, doi: 10.3390/en17246448.

A. Khan, P. Rajendran, and J. S. S. Sidhu, "Passive control of base pressure: A review," *Appl. Sci.*, vol. 11, no. 3, pp. 1–22, 2021, doi: 10.3390/app11031334.

R. Montalà *et al.*, "Deep Reinforcement Learning for Active Flow Control around a Three-Dimensional Flow-Separated Wing at Re = 1,000," no. Ml, pp. 1–12, 2025.

F. Sonkaya, S. Cadirci, and D. Erdem, "Flow Separation Control on NACA0015 Airfoil Using Synchronized Jet Actuator," *J. Appl. Fluid Mech.*, vol. 15, no. 2, pp. 427–440, 2022, doi: 10.47176/jafm.15.02.33068.

A. Krishnan, A. S. M. Al-Obaidi, and L. C. Hao, "A comprehensive review of innovative wind turbine airfoil and blade designs: Toward enhanced efficiency and sustainability," *Sustain. Energy Technol. Assessments*, vol. 60, no. April, p. 103511, 2023, doi: 10.1016/j.seta.2023.103511.

A. Tayebi and F. Torabi, "Flow control techniques to improve the aerodynamic performance of Darrieus vertical axis wind turbines: A critical review," *J. Wind Eng. Ind. Aerodyn.*, vol. 252, no. July, p. 105820, 2024, doi: 10.1016/j.jweia.2024.105820.

O. M. Fouatih, M. Medale, O. Imine, and B. Imine, "Design optimization of the aerodynamic passive flow control on NACA 4415 airfoil using vortex generators," *Eur. J. Mech. B/Fluids*, vol. 56, pp. 82–96, 2016, doi: 10.1016/j.euromechflu.2015.11.006.

W. F. J. Olsman and T. Colonius, "Numerical Simulation of Flow over an Airfoil with a Cavity," *AIAA J.*, vol. 49, no. 1, pp. 143–149, Jan. 2011, doi: 10.2514/1.J050542.

G. C. Y. Lam and R. C. K. Leung, "Aeroacoustics of NACA 0018 Airfoil with a Cavity," *AIAA J.*, vol. 56, no. 12, pp. 4775–4786, Dec. 2018, doi: 10.2514/1.J056389.

T. Durhasan, “Passive Flow Control over an Airfoil by Control Rod at Low Reynolds Number,” vol. 13, no. 6, pp. 1819–1833, 2020.

J. C. Lin, *Review of research on low-profile vortex generators to control boundary-layer separation*, vol. 38, no. 4–5. 2002. doi: 10.1016/S0376-0421(02)00010-6.

S. Uavs and A. Arshad, “Computational Investigations for the Feasibility of Passive Flow Control Devices for Enhanced Aerodynamics of,” 2024.

Y. Xie, Y. Rao, Y. Cheng, and W. Tian, “Investigation into the laminar separation control of airfoils at low Reynolds numbers by dimple vortex generators,” *Aerosp. Sci. Technol.*, vol. 129, p. 107841, 2022, doi: 10.1016/j.ast.2022.107841.

P. B. Sudarsana, J. Singh, and A. Sareen, “Wake Stabilization and Force Modulation via Surface Dimples on an Airfoil at Low-Reynolds-Numbers,” 2025.

E. Sobhani, M. Ghaffari, and M. J. Maghrebi, “Numerical investigation of dimple effects on darrieus vertical axis wind turbine,” *Energy*, vol. 133, pp. 231–241, 2017, doi: 10.1016/j.energy.2017.05.105.

W. F. J. Olsman, J. F. H. Willems, A. Hirschberg, T. Colonius, and R. R. Trieling, “Flow around a NACA0018 airfoil with a cavity and its dynamical response to acoustic forcing,” *Exp. Fluids*, vol. 51, no. 2, pp. 493–509, Aug. 2011, doi: 10.1007/s00348-011-1065-7.



2026 by the authors; Journal of *Kashmir Journal of Academic Research and Development*. This is an open access article distributed under the terms and conditions of the Creative Commons Attribution (CC-BY) license (http://creativecommons.org/licenses/by/4.0/).